ELSEVIER

Magnetic Resonance Imaging 21 (2003) 835–843

MAGNETIC RESONANCE IMAGING

A signal subspace approach for modeling the hemodynamic response function in fMRI

Gholam-Ali Hossein-Zadeh[a], Babak A. Ardekani[b,*], Hamid Soltanian-Zadeh[a,c]

[a]*Electrical and Computer Engineering Department, University of Tehran, Tehran 14399, Iran*
[b]*Nathan Kline Institute for Psychiatric Research, Orangeburg, NY 10962, USA*
[c]*Radiology Department, Henry Ford Hospital, Detroit, MI 48202, USA*

Received 17 January 2003; received in revised form 24 April 2003; accepted 25 April 2003

Abstract

Many fMRI analysis methods use a model for the hemodynamic response function (HRF). Common models of the HRF, such as the Gaussian or Gamma functions, have parameters that are usually selected a priori by the data analyst. A new method is presented that characterizes the HRF over a wide range of parameters via three basis signals derived using principal component analysis (PCA). Covering the HRF variability, these three basis signals together with the stimulation pattern define *signal subspaces* which are applicable to both linear and nonlinear modeling and identification of the HRF and for various activation detection strategies. Analysis of simulated fMRI data using the proposed signal subspace showed increased detection sensitivity compared to the case of using a previously proposed trigonometric subspace. The methodology was also applied to activation detection in both event-related and block design experimental fMRI data using both linear and nonlinear modeling of the HRF. The activated regions were consistent with previous studies, indicating the ability of the proposed approach in detecting brain activation without a priori assumptions about the shape parameters of the HRF. The utility of the proposed basis functions in identifying the HRF is demonstrated by estimating the HRF in different activated regions.

Keywords: Hemodynamic response; fMRI; Analysis; Modeling

1. Introduction

The metabolic processes that accompany neural activity in the brain induce local changes in blood flow, blood volume and tissue oxygenation. The overall result is local variations in the concentration of deoxyhemoglobin which is paramagnetic. This produces variations in the intensity of T_2*-weighted magnetic resonance (MR) images. Based on this fact, functional MR imaging (fMRI) can localize the neural activity by fast acquisition of a series of MR images. Hence fMRI measures a physiologically filtered version of neural activity which is smoothed and delayed by the hemodynamic system. Fig. 1 shows a systematic model of the hemodynamic system as an intermediate mechanism between neural activity and fMRI signal. In many cases, this system is assumed to be linear and time-invariant and its impulse response is denoted as the hemodynamic response function (HRF). Poisson [1], Gamma [2,3], and Gaussian functions [4] are commonly used models for the HRF. Another model proposed by Gossl et al. [5] uses several Gaussian functions for modeling different phases of the HRF. As an example, the Gamma HRF may be parameterized and written in an amplitude normalized form as follows [6]:

$$\mathrm{h}(t;\,\tau,\,\sigma) = \begin{cases} e^{-t/\sqrt{\sigma\cdot\tau}}\left(\dfrac{\mathrm{e}.t}{\tau}\right)^{\sqrt{\tau/\sigma}} & t > 0 \\ 0 & t < 0 \end{cases} \tag{1}$$

The parameter τ represents the location of the peak of the function and the parameter σ influences its width. Fig. 2 shows two families of curves obtained by varying τ and σ independently. These parameters are usually selected a priori by the data analyst. However, it has been shown that the HRF varies significantly between subjects, and within subjects between scanning days [7]. The HRF may also vary between brain regions within a subject. Thus, using a fixed

* Corresponding author. Tel.: +1-845-398-5471; fax: +1-845-398-5472.
E-mail address: ardekani@nki.rfmh.org (B.A. Ardekani).

0730-725X/03/$ – see front matter
doi:10.1016/S0730-725X(03)00180-2

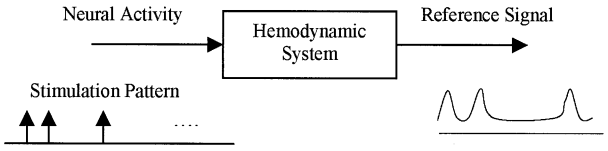

Fig. 1. Modeling the hemodynamic signal from a systematic point of view.

HRF may diminish the sensitivity of activation detection. In addition, if the goal of the study is to investigate the variability of the HRF with respect to various independent variables (e.g., brain site, subject population, field strength), then the results would be biased toward the particular model selected. In this work, we present a method that circumvents the need for a priori selection of these parameters.

The parameters of the HRF model many be treated as extra unknowns to be estimated. However, this usually leads to a difficult nonlinear estimation problem. In this article we propose three basis functions as the basic elements of the HRF. Linear combinations of these bases can cover HRF variability and there is no need for selecting or estimating any nonlinear parameters in this approach. Convolution of these functions with the stimulation pattern forms a signal subspace for linear modeling of the hemodynamic system, which can be used in fMRI analysis. The signal subspace models that have been introduced previously [8] are based on a truncated trigonometric Fourier series and are applicable only to periodic block design fMRI analysis. This signal subspace model cannot be used in event-related fMRI because the stimulation pattern is not periodic. Also in multitask block design experiments, different tasks may have the same period, therefore this model cannot differentiate between their activation signals. In contrast to the previous signal subspaces, the subspace proposed in this paper is applicable in both block design and event-related fMRI.

Recently, the hemodynamic system has been modeled as a nonlinear system [9–11]. Friston et al. [9] presented a model-free characterization of the HRF using nonlinear system identification, namely a Volterra series formulation. In this framework three basis functions where used for expanding the Volterra kernels. The three bases were Gamma functions with different delays that were selected based on previous experimental observations. The basis functions that we introduce in this paper are extracted in a systematic manner and may better represent of hemodynamic behavior.

2. Theory

2.1. Linear time-invariant modeling

As shown in Fig. 1, one can model the vascular coupling of neural activity through a point spread function $h(t)$ also known as the HRF. By considering this linear model one can write:

$$z(t) = h(t) * s(t), \tag{2}$$

where $s(t)$ is the stimulation pattern and $z(t)$ is the expected activation signal. In order to reach a more general model for the signal subspace we focus on the variation of $h(t)$. Assume that all probable realizations of $h(t)$ can be written as linear combinations of a set of basis functions $h_i(t)$. Then using Eq. (2), the measured signal model $z(t)$ can be written as a linear combination of basis vectors $z_i(t)$ as follows:

$$z(t) = \left[\sum_{i=1}^{M} a_i h_i(t)\right] * s(t) = \sum_{i=1}^{M} a_i z_i(t) \tag{3}$$

where

$$z_i(t) = h_i(t) * s(t). \tag{4}$$

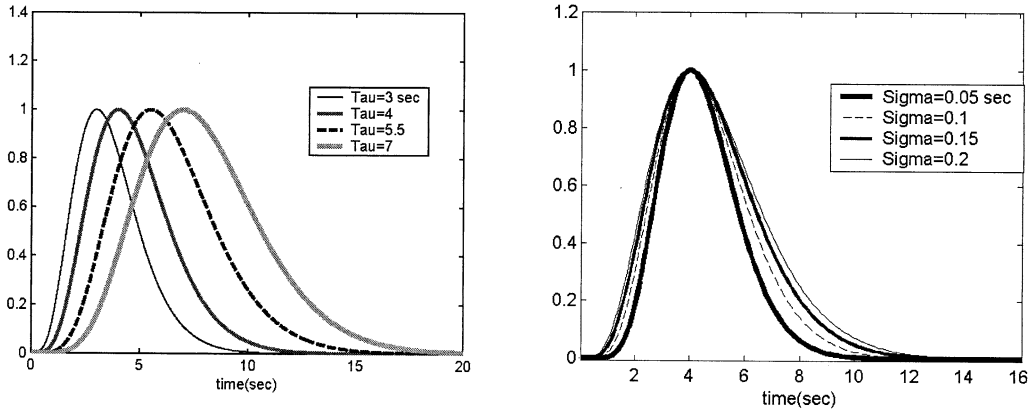

(a) (b)

Fig. 2. Family of Gamma functions obtained for: (a) different τ's (3, 4, 5.5, and 7 s) for $\sigma = 0.15$ s, and (b) different σ's (0.05, 0.1, 0.15, and 0.2 s) for $\tau = 4$ s.

Since the input signal $s(t)$ is always assumed to be the same as the stimulation pattern, only the basis functions $h_i(t)$ need to be defined for computing the basis vectors $z_i(t)$. In other words, if we can define the basis functions $h_i(t)$ such that the HRF, regardless of its exact shape, can be written as a linear combination of $h_i(t)$'s, we can construct a more general signal subspace which may be used in both event-related and block design fMRI data analysis. For finding this basis set, we propose a methodology based on principal component analysis (PCA). Consider a $P\times N_h$ matrix **Q,** containing P different realizations of the HRF, each having N_h time samples. Each row of this matrix contains a realization of the HRF produced by varying the parameters in a class of nonlinear functions, such as the Gamma or Gaussian function, or even by experimental measurements of the HRF. By performing a PCA on $\mathbf{Q}^T\mathbf{Q}$ one can write:

$$\mathbf{Q}^T\mathbf{Q} = \mathbf{H}\mathbf{D}\mathbf{H}^T \tag{5}$$

where $\mathbf{H}$ is an $N_h\times N_h$ matrix containing unit eigenvectors, known as the principal components and $\mathbf{D}$ is a diagonal matrix formed by the eigenvalues $d_{11} \geq d_{22} \geq \ldots \geq d_{N_hN_h}$. The first principal component accounts for as much of the variance in the data as possible, and each succeeding component accounts for as much of the remaining variance as possible. Therefore, the first few eigenvectors are responsible for most of the variance in the data. More precisely, if we choose the first M columns of $\mathbf{H}$ as the desired basis functions $h_i(t)$, we can account for

$$\left(\frac{\sum_{i=1}^{M} d_{ii}}{\sum_{i=1}^{N_h} d_{ii}}\right)\times 100$$

percent of the total variance in the data.

It is obvious that the dimension of the signal subspace is equal to the number of selected eigenvectors M and the basis vectors of the signal subspace, $z_i(t)$, are obtained from (4) by convolving the pattern of stimulation with the selected eigenvectors. Therefore by putting the elements of $z_i(t)$ in an $N\times 1$ vector $\mathbf{z}_i$, the matrix

$$\mathbf{Z} = [\mathbf{z}_1\mathbf{z}_2\ldots\mathbf{z}_M] \tag{6}$$

will contain the bases of the signal subspace for linear modeling of the HRF.

2.2. Application to nonlinear modeling

A model-free and nonlinear characterization of the HRF was introduced by Friston et al. [9] using a Volterra series to describe the input-output relationship of the hemodynamic system. They expanded the unknown kernels of this relationship in terms of a small number of basis functions, which were later selected as three variants of the Gamma function. By this approach the problem of identification (detection) is reduced to a general linear model (GLM), whose design matrix is formed with these three bases and their self- and cross products. As stated by the authors in [9], selecting the three basis functions was motivated by their pervious knowledge of the anticipated hemodynamic response. However, in this study we extracted three basis vectors in a systematic manner such that they may be considered as the best representatives of hemodynamic behavior.

In nonlinear modeling of the HRF a signal subspace can be used which is equivalent to the design matrix in the GLM. The bases of the signal subspace in this case are the basis vectors of linear modeling $z_i(t)$ plus their cross and self-products $y_{ij}(t) = z_i(t)z_j(t)$. Therefore the dimension of this subspace is equal to the number of selected vectors (M) plus the number of their self and cross products M(M+1)2. Therefore the matrix $\mathbf{Z}$ that contains the bases of the signal subspace can be written in a systematic manner similar to the linear case as follows:

$$\mathbf{Z} = [\mathbf{z}_1\mathbf{z}_2\ldots\mathbf{z}_M\mathbf{y}_{11}\mathbf{y}_{12}\ldots\mathbf{y}_{1M}\mathbf{y}_{22}\mathbf{y}_{23}\ldots\mathbf{y}_{2M}\ldots\mathbf{y}_{MM}] \tag{7}$$

3. Material and methods

3.1. Simulated fMRI data

For a realistic simulation of fMRI data, computer generated 'activation' time-series were added to the measured time-series of a single slice of a resting state experimental fMRI data. The resting state fMRI data were collected from a healthy volunteer using a 1.5 Tesla Siemens Vision MRI scanner. Subject wore earplugs and lay comfortably in the scanner with his eyes closed during the experiment. A total of 256 image volumes were scanned using a T_2*-weighted gradient echo single-shot echo-planar (EPI) sequence with TR = 3 sec, TE = 45 ms, Flip Angle = 90°, and FOV = 250 × 250 mm^2. Each volume consisted of 15 transverse slices of size 64 × 64 with a pixel size of approximately 3.91 × 3.91 mm^2 and a slice thickness of 6 mm with no gaps. The first four volumes of this data were discarded, and the remaining volumes were then motion corrected using the AFNI software package (Medical College of Wisconsin, Milwaukee, WI) [12]. The time-series data of a single slice were selected and simulated activation time-series were added to the baseline time-series of voxels corresponding to the predefined spatial pattern shown in Fig. 3(a). The 'activated' areas have different sizes (3, 6, 8, and 12 pixels) and different contrasts (1%, 1.5%, 2%, and 2.5%). The simulated activation time-series consisted of 252 points obtained by convolving of a stimulation pattern with the HRF and then adjusting its amplitude to the desired contrast. The stimulation pattern was a boxcar function with five 150-s

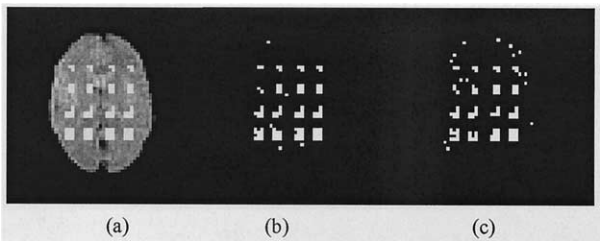

Fig. 3. (a) The spatial pattern of activation in the simulated dataset overlaid on the average image of the dataset. The activation contrasts for the columns (from left to right) are 1%, 1.5%, 2%, and 2.5%, respectively. (b-c) activated areas detected at a false alarm rate of 0.005 using: (b) the proposed subspace; (c) trigonometric subspace.

periods. Each period consisted of 60 s of ON condition followed by 90 s OFF or baseline condition. The HRF was modeled by a gamma function. In order to model the variability of the HRF, the parameters of the gamma function were varied between different activated voxels by randomly selecting the parameters τ and σ between 3 to 7 s and 0.05 to 0.21, respectively. These are in the same range used for deriving the basis functions $h_i(t)$.

3.2. Motor task data (block design)

Functional images were acquired from a normal volunteer using a T_2*-weighted gradient echo single-shot EPI sequence (TR = 3 sec, TE = 50 ms, FOV = 250 × 250 × 100 mm^3, matrix size = 64 × 64 × 20) on a 1.5 Tesla Siemens Vision MRI scanner. The subject performed a finger to thumb opposition task. The task consisted of 4 periods of 84 s, where each period contained 30 s of left hand finger opposition, 12 s of rest, followed by 30 s of right hand finger opposition, and another 12 s of rest. A 3D high-resolution anatomic image volume was also acquired from the subject using a magnetization-prepared rapid acquisition gradient echo (MP-RAGE) sequence.

3.3. Oddball task data (event-related)

Another healthy subject was scanned in another fMRI experiment. The task given to the subject in this experiment is known as the "classic visual oddball paradigm." In this task, a train of equally spaced visual stimuli was presented to the subjects. There were two types of stimuli: the standard stimuli and the target stimuli. The standard events occurred more frequently than the target events. The subject was instructed to count the target stimuli silently and report the total number at the end of the experiment. The standard (frequent) visual stimulus was an image consisting of the string of white characters "OOOOO" on a dark background and occurred 93.36% of the times; the rare (target) image was the string of characters "XXXXX" and occurred 6.64% of the times. A total of 256 images were shown to the subject (17 targets and 239 standards) in one experiment. The target events were distributed randomly among the 256 trials.

Using a single-shot EPI sequence with TR = 1648 ms, TE = 45 ms, Flip Angle = 90°, and FOV = 250 × 250 mm^2, a total of 256 EPI volumes were scanned from the subject. Each volume covered the entire cerebrum and the superior aspect of the cerebellum, consisting of 15 transverse slices of size 64 × 64 with no gaps. The acquisition of each EPI volume was synchronized with the onset of a visual stimulus. In addition to the EPI data, a high-resolution anatomic 3D T_1-weighted image volume was scanned from the subject using an MP-RAGE sequence.

3.4. fMRI data processing steps

As a preprocessing step, the first four volumes of the functional images were discarded and the remaining volumes were motion corrected using the AFNI software package [12]. Linear drifts and mean components were then removed from each voxel time-series.

Let the $N\times1$ column-vector $\mathbf{x}$ represent the time-series measurements of a voxel after the preprocessing step, where N is the number of volumes. For each voxel of the data an F parameter [8] was computed as follows:

$$F = \frac{\mathbf{x}^T\mathbf{P}_z\mathbf{x}/L}{\mathbf{x}^T(\mathbf{I}-\mathbf{P}_z)\mathbf{x}/(N-L-2)}, \tag{8}$$

where $\mathbf{P_z}$ is the *orthogonal projector matrix* of the signal subspace given by

$$\mathbf{P_Z} = \mathbf{Z}(\mathbf{Z}^T\mathbf{Z})^{-1}\mathbf{Z}^T \tag{9}$$

and $\mathbf{Z}$ is an $N\times L$ matrix whose columns are the signal subspace bases, and L is the number of bases vectors. In linear modeling of the HRF $\mathbf{Z}$ is replaced by Eq. (6), while in nonlinear modeling it must be replaced by Eq. (7).

In each voxel we test the null hypothesis "H_0: no activation" against the alternative hypothesis "H_1: the voxel is active." For this purpose we need the probability distribution of F under the null hypothesis which is an F distribution with L and *(N-L-2)* degrees of freedom [8]. Therefore, by choosing a proper false alarm rate α (e.g., $\alpha = 0.0001$) we can find the corresponding threshold F_α from the F distribution and reject H_0 for those voxels with $F \geq F_\alpha$.

4. Results and discussions

4.1. Deriving the basis functions

Before processing any of the images, we used the methodology described in Section 2.1 to derive a signal subspace. Two hundred discrete samples were taken at a rate of 10 samples/s (TR = 0.1 sec) from the Gamma model for the HRF, described by Eq. (1). The procedure described in

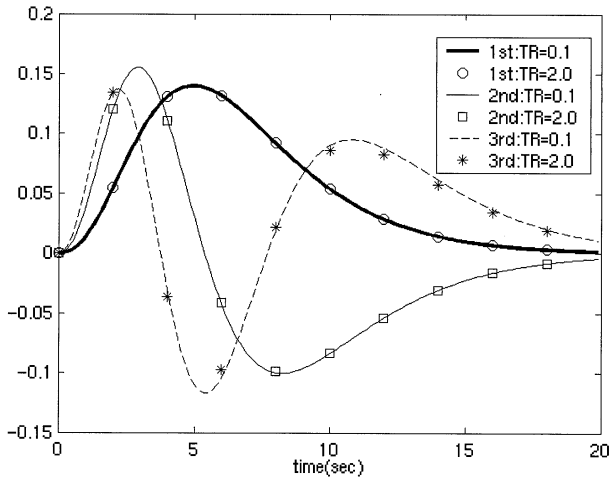

Fig. 4. Three principal components chosen for deriving the signal subspace.

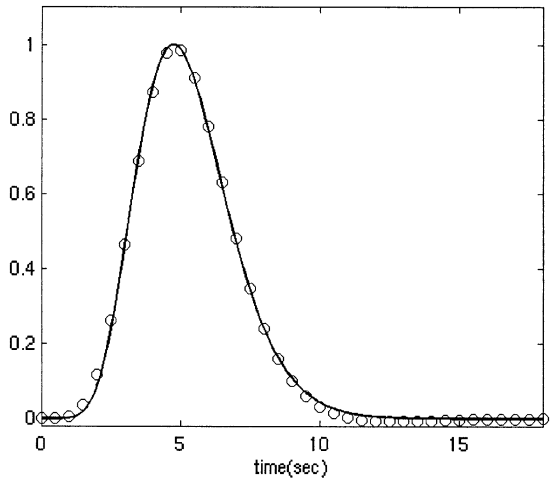

Fig. 5. Approximation of the HRF used in [3] and [13] ($t^b\ exp(-t/c)$, $b = 8.6$, $c = 0.55$) using the basis functions of Fig. 4.

Section 2.1 for deriving a signal subspace requires systematic variation of the model parameters τ and σ over a range that covers probable variations of the actual HRF. Using previously measured values for these parameters in [6], we chose the intervals [3,7] and [0.05, 0.21] for τ and σ, respectively. A total of 300 realizations of the HRF were calculated for different values of τ and σ and put in a 300×200 matrix $\mathbf{Q}$. Principal component analysis of $\mathbf{Q^TQ}$ revealed that the first three eigenvectors are responsible for 99% of the variance in the data matrix $\mathbf{Q}$. This suggests that the first three eigenvectors may be sufficient to form the signal subspace (i.e., $M = 3$). Fig. 4 shows the selected eigenvectors. The basis vectors of the signal subspace for linear model may be obtained by convolving these vectors with the time pattern of stimulation in any fMRI experiment. However, the repetition time TR in fMRI experiments is usually different from 0.1 which was used for deriving these bases. We performed the same procedure for different TRs and observed that the same number of eigenvectors is selected for each TR and also the eigenvectors have the same shape and are only different in a scalar amplitude factor, which is not important in signal subspace modeling. Fig. 4 also shows the selected eigenvectors for TR = 2, concurrent with those selected for TR = 0.1. Various Gamma HRF's used in the literature [3,13] may be closely approximated by linear combinations of these basis signals. An example is shown in Fig. 5. A close agreement exists between our basis functions and those derived by Aguirre et al. [7] by performing SVD on measured experimental data, showing the ability of our basis function to model HRF's in practice. The three components thus identified, together with the stimulation pattern, define *signal subspaces* that can be used in both linear and nonlinear characterization of hemodynamic system and in various activation detection strategies.

4.2. Analysis of simulated fMRI data and comparison study

We convolved the three basis functions obtained in Section 4.1 with the stimulation pattern of the simulated fMRI data in order to obtain the bases of a signal subspace. The procedure discussed in Section 3.4 was used to derive an F map for this data. We compared the performance of the proposed signal subspace for activation detection with that of a previously proposed subspace (trigonometric subspace). The bases of trigonometric subspace were 3 harmonic of sin/cosine pairs of the stimulation frequency (i.e., *sin(ω.t), cos(ω.t), sin(2ω.t), cos(2ω.t), sin(3ω.t), cos(3ω.t)*, where $\omega = 2\pi/150$). Hence the columns of matrix $\mathbf{Z}$ were replaced with time samples from these trigonometric functions, and after deriving $\mathbf{P_z}$ by (9), another F map was computed for the simulated data. These F maps were then thresholded for different false alarm rates and true detections of methods were measured. Figs. 3(b) and (c) show the detected areas of activation at false alarm rate of 0.005 using the two subspaces, demonstrating the superior sensitivity of the proposed subspace over the trigonometric subspace. Fig. 6 graphs the number of true positives of two methods at different false alarm rates. This graph indicates that using the proposed subspace improves the detection sensitivity when the HRF varies for different activated areas.

4.3. Analysis of the motor data

The three basis functions obtained in Section 4.1 were convolved with the stimulation pattern of the motor task in order to obtain the bases of a signal subspace. The procedure discussed in Section 3.4 was used for detecting any activation corresponding to the right hand finger opposition in the motor data. Three functional areas that have been reported consistently in literature [14–16] were found active

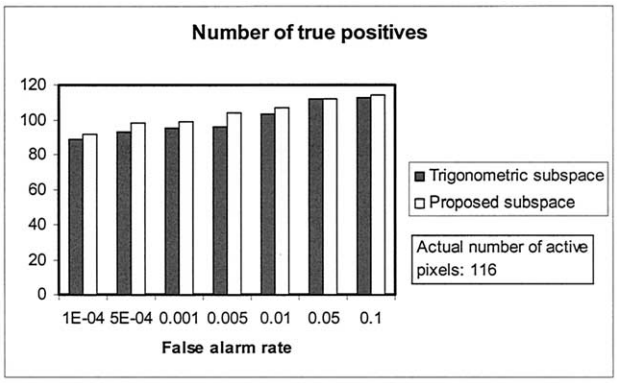

Fig. 6. Comparison of the number of correctly detected active voxels (true positives) in the simulated data using the proposed subspace and the trigonometric subspace.

by using the proposed signal subspace. Fig. 7 shows three different slices from activations obtained at a false alarm rate of 0.005, overlaid on registered anatomic images in the AFNI visualization software. A filter was applied to the results that removed isolated single activated voxels, which are mostly false alarms. As expected, activation has been detected in the left primary motor cortex and the right cerebellum and supplementary motor area. Also the motor data were reanalyzed by nonlinear modeling of the HRF. Fig. 8 shows the same slices of activated areas for a false alarm rate of 0.005. In this task and for this subject no significant differences were observed between activation areas found by linear modeling of the HRF versus nonlinear modeling, in the sense that both were able to detect the expected active regions.

4.4. Analysis of the oddball task data

The three basis functions obtained in Section 4.1 were convolved with the stimulation pattern of the oddball paradigm to form the signal subspace for this data. Then the procedure of Section 3.4 was used for detecting activated areas. The activated areas detected in this paper with a false alarm rate of 0.00001 were consistent with the literature [17–18], including left inferior parietal lobule (Broadman Area 40 or BA40), bilateral superior parietal lobule (BA 7), left cerebellum, insula, and anterior cingulate gyrus (BA 24). Fig. 9 shows some of these areas in three different

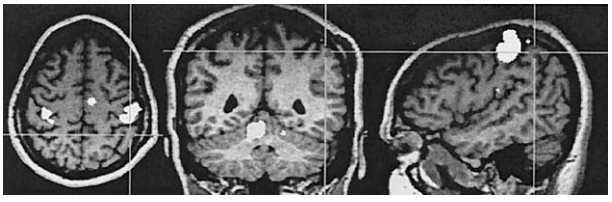

Fig. 7. Activated brain regions in a right hand finger to thumb opposition task detected by using the proposed signal subspace in the case of linear modeling of HRF.

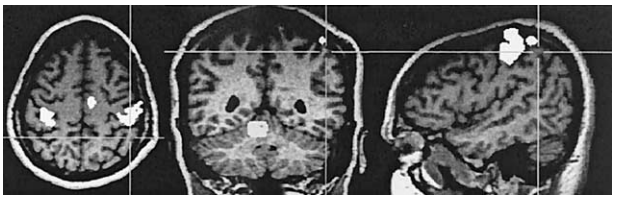

Fig. 8. Activated brain regions in a right hand finger to thumb opposition task detected by using the proposed signal subspace for nonlinear modeling of HRF.

slices overlaid on registered anatomic images in AFNI visualization software. In order to demonstrate the ability of the proposed basis functions in modeling different HRF shapes, we plotted the estimated HRF for some of the activated regions. In fact at each voxel we fit the model $\mathbf{x} = \mathbf{Z}\beta + \mathbf{n}$, where $\mathbf{x}$ is the voxel time-series, $\mathbf{Z}$ is the matrix that contains the basis vectors of the signal subspace, β is the vector of unknown coefficients, and $\mathbf{n}$ is the vector of residuals treated as noise. By obtaining a least square (LS) estimation of β for an active voxel, one can approximate the HRF at that voxel by $\sum_{i=1}^{M} \beta_i h_i(t)$,where $h_i(t)$'s are the elementary functions derived in Section 4.1. By averaging the HRF estimations over different voxels of an activated region, it is possible to drive an estimate of the HRF for the region. Fig. 10 shows the estimated HRF in left inferior parietal lobule, anterior cingulate gyrus, and left cerebellum. These figures demonstrate that the HRF shape differs for different regions.

4.5. Relationship between the three basis functions and the Taylor series

The derivatives of a multi parameter function with respect to its parameters can be used through the Taylor series for approximating the function for different values of parameters. The hemodynamic response function (HRF) used in this paper, $h(t; \tau, \sigma)$, has two parameters σ and τ corresponding to its shape and time shift. Therefore, using a Taylor series one can write:

$$h(t;\, \tau_0 + \tau,\, \sigma_0 + \sigma) \approx h(t;\, \tau_0,\, \sigma_0) + \tau.\frac{\partial h(t;\, \tau,\, \sigma)}{\partial \tau}\bigg|_{\tau=\tau_0,\sigma=\sigma_0} \tag{10}$$

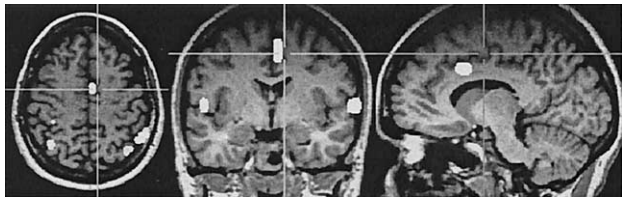

Fig. 9. Activated brain areas in the oddball paradigm detected using the linear modeling of HRF with the proposed subspace.

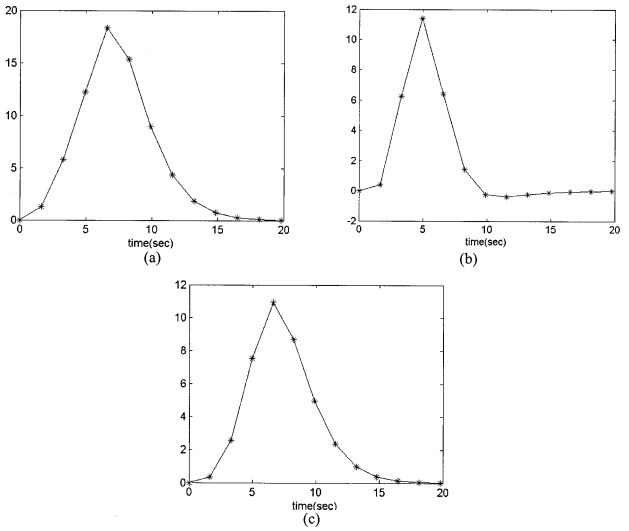

Fig. 10. Estimated hemodynamic response for different active areas (averaged on that area); (a) inferior parietal lobule; (b) anterior cingulate gurus; (c) cerebellum.

$$+\ \sigma\ \frac{\partial h(t;\ \tau,\ \sigma)}{\partial \sigma}\bigg|_{\tau=\tau_0,\sigma=\sigma_0}.$$

Thus, different variations of the HRF can be approximated as a linear combination of three basis functions $h(t;\ \tau_0,\ \sigma_0)$,. $\frac{\partial h(t;\tau,\sigma)}{\partial \tau}\Big|_{\tau=\tau_0,\ \sigma=\sigma_0}$, and $\frac{\partial h(t;\tau,\sigma)}{\partial \sigma}\Big|_{\tau=\tau_0,\sigma=\sigma_0}$.

The equations below show the derivatives of the Gamma function stated in Eq. (1) with respect to the parameters.

$$\frac{\partial h}{\partial \tau} = e^{-\frac{t}{\sqrt{\sigma.\tau}}}.\left(\frac{et}{\tau}\right)^{\sqrt{\frac{\tau}{\sigma}}}.\left(\frac{1}{\sqrt{\tau.\sigma}}\right) \cdot\left[\frac{t}{2.\tau}+\frac{1}{2}\ln\left(\frac{et}{\tau}\right)-1\right] \tag{11}$$

$$\frac{\partial h}{\partial \sigma} = e^{-\frac{t}{\sqrt{\sigma.\tau}}}.\left(\frac{et}{\tau}\right)^{\sqrt{\frac{\tau}{\sigma}}}.\left(\frac{1}{2\sigma\sqrt{\sigma}}\right) \cdot\left[\frac{t}{\sqrt{\tau}}-\ln\left(\frac{et}{\tau}\right).\sqrt{\tau}\right] \tag{12}$$

We assessed the relationship of three principal components we obtained using PCA with those above. The first principal component is well approximated by a Gamma function with parameters $\tau = 5.2$, $\sigma = 0.18$. Fig. 11a shows the first principal component plotted against this Gamma function. The derivatives of the Gamma function with respect to τ and σ (stated by Eq. (11) and (12)) are also plotted against the second and third principal components in Figs. 11b and 11c, respectively. From these figures it can be seen that the basis functions that we derived by PCA are close to those provided by Taylor series, but they are not equal. Given that PCA analysis ensures that the components are orthogonal, a necessary condition for the second and third components being $\partial h/\partial\sigma$ and $\partial h/\partial\tau$ is that they are orthogonal to $h(t)$, that is:

$$\int_0^\infty h(t)\ \frac{\partial h(t)}{\partial \sigma}\ dt = 0 \tag{13}$$

and

$$\int_0^\infty h(t)\ \frac{\partial h(t)}{\partial \tau}\ dt = 0. \tag{14}$$

Since the analytical assessment of the above questions is complex and out of the scope of this work, we examined them by a numerical integration in MATLAB [Mathworks Inc.] where we obtained the results $\int_0^\infty h(t)\ \frac{\partial h(t)}{\partial \tau}\ dt = 0.3053$,and $\int_0^\infty \mathrm{h(t)}\ \frac{\partial \mathrm{h(t)}}{\partial \sigma}\ \mathrm{dt}=2.36705$. These results indicate that the second and third principal components cannot be the derivatives of a Gamma function.

In conclusion, the Taylor series also provides a set of basis functions for approximating the HRF in this case, but is not as general as PCA. PCA is a nonparametric approach that can be used even for experimentally measured data, while Taylor series can only be used for parametric approaches, where the partial derivatives of HRF can be computed with respect to its parameters analytically.

5. Conclusion

Taking advantage of PCA and using different realizations of HRF, three basis functions were derived as representatives of the HRF. Covering HRF variability, these three basis signals together with the stimulation pattern define *signal subspaces* which are applicable in both linear and nonlinear modeling and identification of HRF and for various activation detection strategies. They were applied for activation detection in both event-related and block design experimental fMRI data and also in both linear and nonlinear modeling of HRF. The activated regions were consistent with previous studies, indicating the capability of this approach for detecting activated brain regions without a priori assumptions about the shape parameters of the HRF. We used simulated fMRI data to demonstrate increased sensitivity of the proposed signal subspace to detect activation areas relative to the previously proposed trigonometric subspace. The ability of the proposed basis functions for HRF identification was demonstrated by estimating the HRF in several activated regions. Therefore this approach may be used for studying the variability of the HRF in different brain regions without biasing the results toward a predefined HRF.

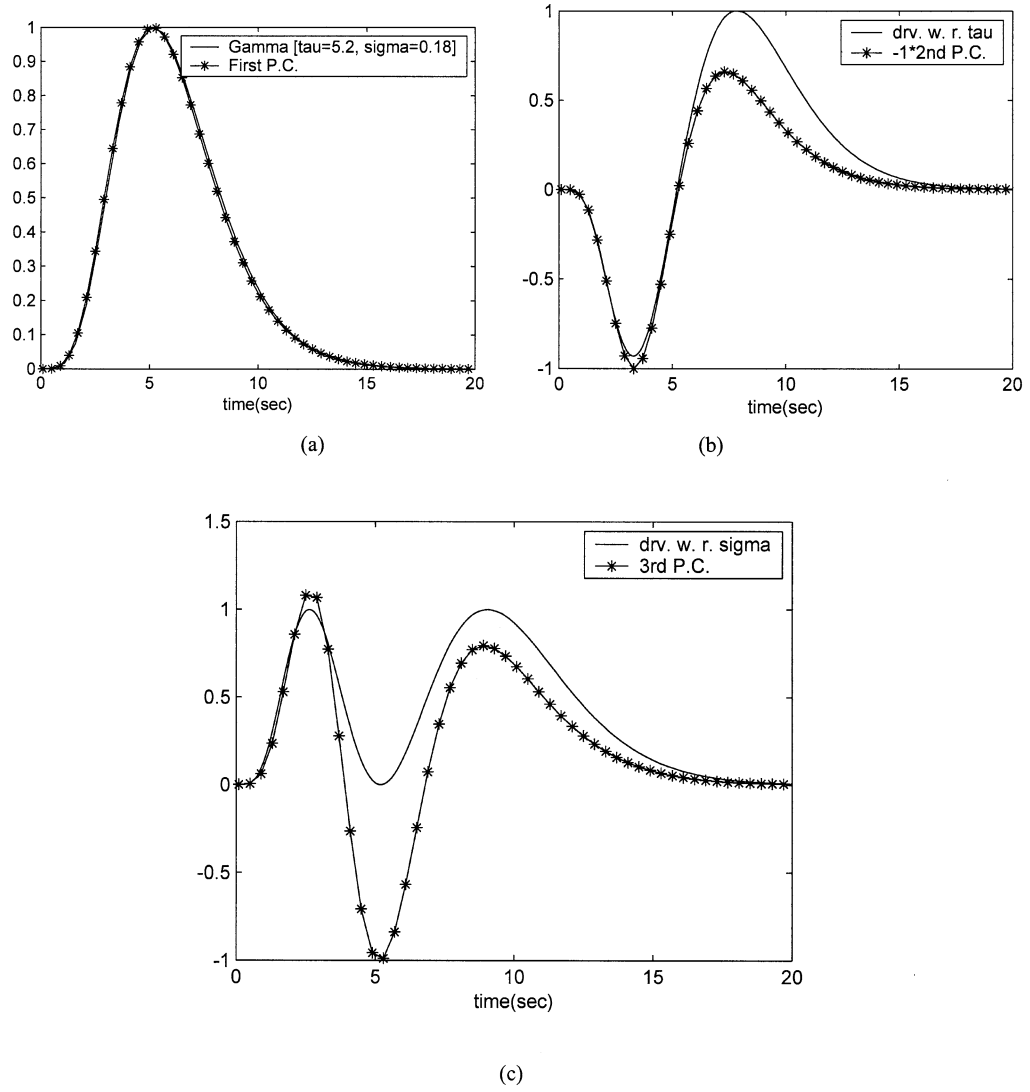

Fig. 11. (a) The first principal component plotted against a Gamma function. (b) derivative of the Gamma function with respect to τ, plotted against the second principal component. (c) derivative of the Gamma function with respect to σ, plotted against the third principal component.

References

[1] Friston KJ, Jezzard P, Turner R. Analysis of functional MRI time-series. Human Brain mapping 1994;1:153–71.

[2] Boyton GM, Engel SA, Glover GH, David JH. Linear systems analysis of functional magnetic resonance imaging in human V1. The Journal of Neuroscience 1996;16:4207–21.

[3] Cohen MS. Parametric analysis of fMRI data using linear systems methods. NeuroImage 1997;6:93–103.

[4] Kruggel F, Von Cramon DY. Modeling the hemodynamic response in single-trial functional MRI experiments. Magn Reson Med 1999;42: 787–97.

[5] Gossl C, Fahrmeir L, Auer D. P. Baysian modeling of the hemodynamic response function in BOLD fMRI. NeuroImage 2000;14:140–8.

[6] Knuth KH, Ardekani BA, Helpern JA. Bayesian estimation of a parameterized hemodynamic response function in an event-related fMRI experiment. Proc. of ISMRM 2001;3:1732.

[7] Aguirre GK, Zarahn E, D'Esposito M. The variability of human BOLD hemodynamic responses. Neuroimage 1998;8:360–9.

[8] Ardekani BA, Kanno I. Statistical methods for detecting activated regions in functional MRI of the brain. Magn Reson Imag 1998;16: 1217–25.

[9] Friston KJ, Josephs O, Rees G, Turner R. Nonlinear event-related response in fMRI. Magn Reson Med 1998;39:41–52.

[10] Friston KJ, Mechelli A, Turner R, Price CJ. Nonlinear responses in fMRI: The balloon model, Volterra kernels, and other hemodynamics. NeuroImage 2000;12:466–77.

[11] Buxton RB, Wong EC, Frank LR. Dynamics of blood flow and oxygenation changes during brian activation: The balloon model. Magn Reson Med 1998;39:855–64.

[12] Cox RW, Hyde JS. Software tools for analysis and visualization of fMRI data. NMR Biomed 1997;10:171–8.

[13] Bandettini PA, Cox RW. Event-related fMRI contrast when using constant interstimulus interval: Theory and experiment. Magn Reson Med 2000;43:540–8.

[14] Moritz CH, Meyerand ME, Cordes D, Haughton VM. Functional MR imaging activation after finger tapping has a shorter duration in the basal ganglia than in the sensorimotor cortex. American Journal of Neuroradiology 2000;21:1228–34.

[15] Moritz CH, Haughton VM, Cordes D, Quigley M, Meyerand ME. Whole brain functional MR imaging activation from a finger tapping task examined with independent component analysis. American Journal of Neuroradiology 2000;21:1629–35.

[16] Joliot M, Papathanassiou D, Mellet E, Quinton O, Mazoyer N, Courtheoux P, Mazoyer B. FMRI and PET of self-Paced finger movement: comparison of intersubject stereotaxic averaged data. NeuroImage 1999;10:430–47.

[17] Ardekani BA, Choi SJ, Hossein-Zadeh GA, Porjesz B, Tanabe JL, Lim KO, Bilder R, Helpern JA, Begleiter H. Functional magnetic resonance imaging of the visual P300 event-related potential. Cognitive Brain Research 2002;14:347–56.

[18] Linden DEJ, Prvulovic D, Formisano E, Völlinger M, Zanella FE, Goebel R, Dierks T. The functional neuroanatomy of target detection: an fMRI study of visual and auditory oddball tasks. Cereb Cortex 1999;9:815–23.